JOURNAL OF COMPUTATIONAL PHYSICS 45, 345–366 (1982)

Orbit-Averaged Implicit Particle Codes*

BRUCE I. COHEN AND ROBERT P. FREIS

Lawrence Livermore National Laboratory, University of California, Livermore, California 94550

AND

VINCENT THOMAS

Electronics Research Laboratory, University of California, Berkeley, California 94720

Received July 30, 1981; revised November 19, 1981

The merging of orbit-averaged particle code techniques with recently developed implicit methods to perform numerically stable and accurate particle simulations are reported. Implicitness and orbit averaging can extend the applicability of particle codes to the simulation of long time-scale plasma physics phenomena by relaxing time-step and statistical constraints. Difference equations for an electrostatic model are presented, and analyses of the numerical stability of each scheme are given. Simulation examples are presented for a one-dimensional electrostatic model. Schemes are constructed that are stable at large-time step, require fewer particles, and, hence, reduce input–output and memory requirements. Orbit averaging, however, in the unmagnetized electrostatic models tested so far is not as successful as in cases where there is a magnetic field. Methods are suggested in which orbit averaging should achieve more significant improvements in code efficiency.

1. INTRODUCTION

Significant progress has recently been achieved in extending the applicability of particle codes to the study of long time-scale plasma physics phenomena [1–5]. Particle simulation has long been a reliable and versatile tool for studying plasma kinetic phenomena. Numerical stability of conventional particle codes, however, had previously required temporal resolution of high-frequency normal modes. For example, the integration time step Δt had to satisfy $\omega_{pe}\Delta t < 2$ (where ω_{pe} is the electron plasma frequency) or satisfy a Courant condition (i.e., $\Delta x/\Delta t$ must be greater than the wave phase velocity). In laboratory and naturally occurring plasmas, the global dynamical time scales of most interest, e.g., those on which particle and energy

* This work was performed under the auspices of the U. S. Department of Energy at the Lawrence Livermore National Laboratory under Contract W-7405-ENG-48 and at the University of California, Berkeley, under Contract DE-AT03-76ET53064-DE-AM03-76SF00034.

0021-9991/82/030345-22$02.00/0

transport or low-frequency instabilities occur, are often many orders of magnitude longer than those associated with the highest-frequency normal modes. Therefore, application of particle simulation to the study of such plasmas is severely limited. The inventions described in [1–5] greatly relax conventional time-step constraints and generally allow use of much larger time steps.

There are major differences in the philosophy and mechanics of the various techniques presented in [1–5]. A few general comments are given here in this introduction with a more detailed critique furnished in the body of the paper.

In [1], an orbit-averaged particle code was presented. This scheme introduced a short time scale, on which particle trajectories were accurately integrated and the plasma currents were accumulated on a spatial grid. On a much longer time scale, plasma currents were time-averaged, and Maxwell's equations were solved in a magneto-inductive approximation using an explicit predictor–corrector scheme. With the introduction of numerical filtering and damping, stable and well-behaved simulations were performed. The two principal gains of this method were (1) the relaxation of the Courant condition associated with Alfvén wave propagation, and (2) the reduction of the simulation particles required for an adequate description of the phase-space distribution function and a tolerable level of fluctuations. These gains in computational leverage have allowed realistic two-dimensional simulation of mirror-machine buildup and confinement spanning five orders of magnitude in time scales going from the ion-cyclotron period to the neutral-beam, charge-exchange replacement time and ion-electron slowing-down time [1].

In the other computational approaches described in [2–5], the field equations and plasma equations of motion have been differenced and solved implicitly. Moment equations describing conservation of mass and momentum are introduced in the schemes given in [2–4] as intermediaries between the particle equations of motion and Maxwell's equations; the latter require the plasma number and current densities n and $\mathbf{J}$ as sources for the fields. Because of the presence of the electric field in the momentum conservation law, the fluid equations provide prescriptions for n and $\mathbf{J}$, whose implicit dependence on the electric field is both linear and easily exhibited. Coupling of the moment equations to the particles is maintained by using particle data for the kinetic stress tensor and for the explicit values of n and $\mathbf{J}$ needed from previous time levels.

Reference [5] offers a qualitatively different and more direct implicit scheme in which the trajectory of the particles are Taylor-series expanded to exhibit their dependence on the acceleration and, hence, on the electric and magnetic fields seen along their paths. The resulting modifications to n and $\mathbf{J}$ are assumed small compared to their corresponding free-streaming values, thus allowing linearization of the dependence of n and $\mathbf{J}$ on the fields. Solution for the fields is then obtained by inversion of a sparsely banded matrix. These implicit schemes relax stability constraints on time step set by waves.

Time-step constraints required for stable and accurate integration of the particle trajectories in both orbit averaging and implicit methods remain. In particular, it is required in the unmagnetized implicit electrostatic models that $|k_{max} v \Delta t| < 1$ and

$|k_{max} a \Delta t^2| < 1$, where k_{max} is the maximum spatial wavenumber retained, Δt is the time step, and v and a are the particle velocity and acceleration. These constraint conditions can still influence the practicality of simulating very slowly evolving collective plasma phenomena, and simulations with realistic parameters using these implicit methods on the most advanced computers may still be too expensive.

Because the product of the number of particles with the number of time steps usually governs the total cost of a simulation, orbit averaging is attractive. When successful, orbit averaging can achieve a large reduction in the requisite number of simulation particles and allows (depends on) time splitting of different modules in the simulation algorithm to more efficiently track phenomena with disparate time scales. The reduction in particles results from sampling the contributions of a single particle to n and $\mathbf{J}$ at many discrete positions along its phase–space trajectory and then time averaging these contributions before solving Maxwell's equations for the new self-consistent fields. In a sense, the many discrete phase–space positions of the single particle used in the averaging are equivalent to many more discrete particles. This has been exploited to great advantage in earlier steady-state simulations [6] and in time-dependent, orbit-averaged simulations [1].

This paper examines the merging of orbit averaging with the recently developed implicit particle-code methods. We wish to combine the robust stability characteristics of the implicit methods with the savings in particle number that may be possible with orbit averaging. By means of analytical derivation of simple dispersion relations describing the numerical stability of various time-differencing schemes and with a few corroborating simulation examples, we demonstrate how orbit averaging can be combined with the moment-equation, field-implicit method [2–4] or the direct-particle and field-implicit scheme [5] to give stable algorithms at large time step. We also prove that simple orbit averaging, which is explicit and iterative, leads to an unstable electrostatic algorithm but can be used to give a stable magneto-inductive code (see companion paper [7]).

We emphasize that there is enormous room for invention in synthesizing differencing schemes for implicit and orbit-averaged simulation algorithms. Although we offer a few guiding principles that should improve the likelihood of achieving numerical stability at large time step, the numerical stability, filtering, and accuracy characteristics of each class of schemes should be determined on a case-by-case basis. Our most important conclusion is that successful orbit averaging requires a distinct separation of time scales between the particle trajectory time scale and a longer time scale for the evolution of the average distribution function and the electromagnetic fields.

The remainder of the paper is organized as follows. In Section 2, we shall present the design and analysis of a number of different orbit-averaged and implicit differencing schemes. We specialize our considerations to simple one-dimensional electrostatic models with no externally applied magnetic field. Simulation results obtained with the one-dimensional electrostatic code ES1 [8] are described in Section 3. A discussion and summary are given in Section 4.

2. Design and Analysis of Orbit-Averaged and Implicit Particle Codes

In this section we shall introduce a number of model differencing schemes for electrostatic physics models and analyze their numerical stability characteristics by deriving the cold plasma dispersion relation for each. This is closely akin to the simple harmonic oscillator analysis described in [9]. The stability analysis is relatively simple but is new and decidedly non-trivial because of orbit averaging and the predictor–corrector approach; it is a highly reliable tool that has guided our design of new algorithms and has assisted us in understanding the numerical instability or damping characteristics of our simulations.

2.1. *Stability*

The very simplest simulation model is a one-dimensional electrostatic model with no magnetic field. This model has been extended to the large time step ($\omega_{pe}\,\Delta t \gg 1$) in [2, 3, 5] by implementing an implicit solution of Poisson's equation relating the electric field to the induced charge density in the plasma. Motivated by the success of the scheme reported in [1], we begin with an analysis of an explicit predictor–corrector, orbit-averaged electrostatic model. This algorithm is unstable but can be stabilized with the introduction of sufficient implicitness.

A simple, orbit-averaged electrostatic model is given by the difference equations

$$(D_x/2)(E^{M+1} + E^M) = 4\pi q(\langle n\rangle^{M+1/2} - n_0), \tag{1}$$

$$x^{j+1} - x^j = v^{j+1/2}\,\Delta t, \tag{2}$$

$$v^{j+1/2} - v^{j-1/2} = (q/m)\,E^*\,\Delta t, \tag{3}$$

where D_x is the spatial derivative operator; E is the electric field known only at macro-time levels denoted by M and $M+1$; x and v are particle positions and velocities known at small or micro-time levels denoted by j; $\langle n\rangle$ is the orbit-averaged charge density

$$\langle n\rangle^{M+1/2} = \frac{1}{N+1}\sum_{j=0}^{N}\sum_{i} S(x_i^j - x); \tag{4}$$

$S(x_i^j - x)$ is the standard particle shape and interpolation factor [7]; i is the particle index; $0 \leqslant j \leqslant N$ corresponding to $M\,\Delta T \leqslant (t = M\,\Delta T + j\,\Delta t) \leqslant (M+1)\,\Delta T$; $N \equiv \Delta T/\Delta t$ the ratio of macro- to micro-time step; and

$$E^* = E^M \qquad \text{(predictor)} \tag{5a}$$

$$= \alpha E^{M+1} + (1-\alpha)\,E^M \qquad \text{(corrector)}, \tag{5b}$$

which is interpolated from the grid to the particle using $S(x_i^j - x)$.

In Fig. 1, we present a schematic showing the separation of micro- and macro-time levels and the leap-frog time advance of the code variables. The particles are

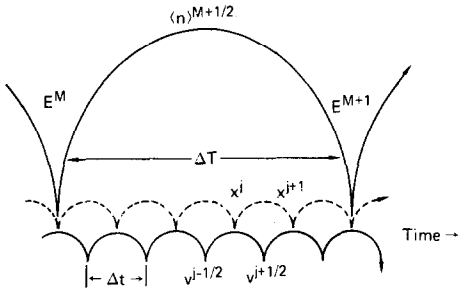

FIG. 1. Schematic of orbit averaging in simplest one-dimensional electrostatic model. Note that $\langle n \rangle$ is averaged in time over densities accumulated at each micro-time step.

advanced first in a predictor step with Eqs. (2) and (3), and E^* is given by the previous time-level value E^M. Gauss' law (Eq. (1)) is used with the average $\langle n \rangle$ to determine a predictor estimate of E^{M+1}, which is then used in Eq. (5b) for E^*. Note that α is a temporal biasing parameter $0 \leqslant \alpha \leqslant 1$. The particles are returned to their former phase–space positions at $t = M\Delta T$ and then advanced with Eqs. (2) and (3) to $t = (M+1)\Delta T$ again in the corrector step to determine an improved value of $\langle n \rangle^{M+1/2}$ and, hence, E^{M+1}.

This explicit predictor–corrector advance of the field and particle equations is numerically unstable to a temporal instability. For purposes of simplifying the analysis, we assume a linear disturbance of a cold, uniform, non-drifting plasma and ignore spatial grid effects ($\Delta x \to 0$). The perturbed particle velocity and position are given by

$$v^{j+1/2} = v^{1/2} + (q/m)\, j \Delta t E^*, \tag{6a}$$

$$x^j = x^0 + v^{1/2} j \Delta t + (q/2m) j(j-1) \Delta t^2 E^*. \tag{6b}$$

The averaged linear density perturbation is

$$\langle n \rangle^{M+1/2} - n_0 = -\frac{\partial}{\partial x}\left(n_0 \sum_0^N x^j/(N+1)\right)$$

$$\approx -\frac{\partial}{\partial x}\left[n_0\left(x^M + \frac{\Delta T}{2} v^M + \frac{q\,\Delta T^2}{2m} E^*\right)\right]. \tag{7}$$

We have employed the summation formulae

$$\sum_{j=0}^{N} j = N(N+1)/2, \qquad \sum_{j=0}^{N} j^2 = N(N+1)(2N+1)/6,$$

have assumed that $N \gg 1$, and have denoted (x^M, v^M) as the values of x^j and $v^{j+1/2}$ nearest to the beginning of the macro interval.

With substitution of $\langle n\rangle^{M+1/2} - n_0$ from Eq. (7) with $E^* = E^M$ into Eq. (1) and Fourier analysis in space, we obtain the predicted value

$$E^{M+1} = -\left(1 - \frac{\omega_p^2 \Delta T^2}{3}\right) E^M - 8\pi n_0 q \left(x^M + \frac{\Delta T}{2} v^M\right). \tag{8}$$

E^* on the corrector pass is given by substituting Eq. (8) into Eq. (5b). We then use Eqs. (6) and (7) to recalculate x, v, and $\langle n\rangle - n_0$ and obtain

$$x^{M+1} - x^M = \frac{\Delta T}{2}(v^{M+1} + v^M), \tag{9a}$$

$$v^{M+1} - v^M = q\frac{\Delta T}{m} E^*$$

$$= q\frac{\Delta T}{m}\left(\alpha\left[-\left(1 + \frac{\omega_p^2 \Delta T^2}{3}\right) E^M - 8\pi n_0 q \left(x^M + \frac{\Delta T}{2} V^M\right)\right] + (1-\alpha) E^M\right) \tag{9b}$$

$$\tfrac{1}{2}(E^{M+1} + E^M) - \frac{\omega_p^2 \Delta T^2}{6}\left(1 + \frac{\omega_p^2 \Delta T^2}{3}\right) E^M$$

$$= -4\pi n_0 q \left(1 - \frac{\omega_p^2 \Delta T^2}{3}\right)\left(x^M + \frac{\Delta T}{2} v^M\right). \tag{9c}$$

Introduction of the Fourier representation, $(x^M, v^M, E^M) = (\tilde{x}, \tilde{v}, \tilde{E})\, z^M$ + c.c., where $z \equiv \exp(-i\omega \Delta T)$, and algebraic reduction of Eqs. (9a)–(9c) give a dispersion relation. The most strongly backward-differenced (forward-biased) scheme and the least unstable for $\alpha \leqslant 1$ corresponds to $\alpha = 1$. If we define $R \equiv \omega_p^2 \Delta T^2$, then the dispersion relation for $\alpha = 1$ can be expressed as the cubic equation

$$[(z-1)^2 + 2Rz]\left(z + 1 - \frac{R}{3} - \frac{R^2}{9}\right) - 2Rz\left(1 - \frac{R^2}{9}\right) = 0. \tag{10}$$

For $R = \omega_p^2 \Delta T^2 \ll 1$, the plasma oscillation is recovered at lowest order in R, giving two normal modes

$$(z-1)^2/z = -R \quad \rightarrow \quad \omega^2 = \omega_p^2, \tag{11}$$

which are weakly damped at next order in $\omega_p \Delta T$. The third normal mode oscillates at the Nyquist frequency ($\omega = \pi/\Delta T$) and is weakly unstable

$$z = -1 - R/6. \tag{12}$$

For $R = \omega_p^2 \Delta T^2 \gg 1$, the highest power of R in Eq. (10) is R^2. Setting the coefficients of R^2 equal to zero gives a quadratic which has one damped and one unstable solution

$$z_\pm = -2 \pm \sqrt{3}. \tag{13}$$

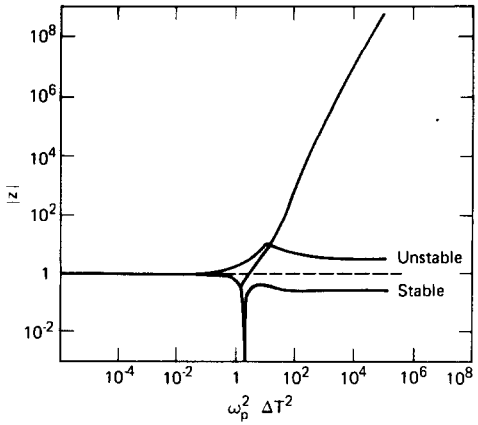

FIG. 2. Absolute value $|z| = |\exp(-i\omega\,\Delta T)|$ as a function of $\omega_p^2 \Delta T^2$ for an explicit predictor–corrector, orbit-averaged electrostatic algorithm. There is weak instability for $\omega_p^2 \Delta T^2 \ll 1$ and strong growth for $\omega_p^2 \Delta T^2 > 1$.

The third root of Eq. (10) is even more unstable when $R \gg 1$, for which

$$z \approx R^2/9. \tag{14}$$

In Fig. 2, we exhibit the general numerical solution of Eq. (10) for the most unstable normal mode. For $\omega_p^2 \Delta T^2 < 1$, there is, indeed, weak instability; at larger time steps, the algorithm is unstable for all values of α, $0 \leqslant \alpha \leqslant 1$, and the growth rates are large.

All of the analyses presented in this section are directly applicable to a hybrid quasi-neutral electrostatic model. We adopt a Boltzmann response for the electrons, assuming that they are isothermal, and model the ions as particles. The quasi-neutrality condition is

$$n_i = n_e = n_0 \exp(e\phi/T_e),$$

from which follows the electric field

$$E = -\partial\phi/\partial x = -(\bar{T}_e/e)(\partial/\partial x) \ln(\langle n_i \rangle / n_0), \tag{15}$$

where the angular bracket indicates the introduction of orbit averaging. This equation replaces Eq. (1). The linear ion-density perturbation is given by $n_i^{(1)} = -\partial(n_0 x^{(1)})/\partial x$, from which the linear electric field is determined by Eqs. (15) and (7). We assume the unperturbed plasma to be uniform. The only change in the resulting linear dispersion relations is the replacement of ω_p^2 with $k^2 c_s^2 \equiv k^2 T_e/m_i$, which indicates that the normal modes are now ion-acoustic waves.

We next consider stabilizing modifications of the electrostatic algorithm. Motivated by the success of implicit schemes, we replace Eq. (5) with $E^* = \alpha E^{M+1} + (1-\alpha) E^M$ and suppose that the corrector iterations have converged or an actual implicit field

solve is performed, as in [5]. Linearizing and Fourier analyzing Eqs. (6) and (7) yield the dispersion relation

$$(z+1)(z-1)^2 + \left(\frac{\omega_p^2 \Delta T^2}{3}(z^2+4z+1)(\alpha z+1-\alpha)\right) = 0. \tag{16}$$

The plasma oscillation is again recovered for $\omega_p^2 \Delta T^2 \ll 1$; at large time step $\omega_p^2 \Delta T^2 \gg 1$, the normal modes are described by $z = -(1-\alpha)/\alpha$ and $z = -2 \pm \sqrt{3}$. Thus, the electrostatic algorithm continues to be unstable at large time step.

Stable orbit-averaged implicit electrostatic schemes do exist, however. Consider the following scheme that is an example of a direct-particle and field-implicit scheme [5]. We replace Gauss' law (Eq. (1)) with the equivalent relation in one dimension,

$$(\partial E/\partial t) + 4\pi J = 0,$$

and difference it as

$$(E^{M+1} - E^M)/\Delta T + 4\pi \langle J \rangle^{M+1/2} = 0, \tag{17}$$

where

$$\langle J \rangle^{M+1/2} = \frac{1}{N+1} \sum_{j=0}^{N} \sum_i q \frac{v_i^{j+1/2}}{2} [S(x_i^j - x) + S(x_i^{j+1} - x)] \tag{18}$$

and Eqs. (2) and (3) describe the particle motion. The averaging interval in Eq. (18) extends from $t = M\Delta T$ to $t = (M+1)\Delta T$ and is centered at $(M+1/2)\Delta T$. For E* in Eq. (3), we employ $E^* = \alpha E^{M+1} + (1-\alpha) E^M$.

To guarantee that $\langle J \rangle^{M+1/2}$ is implicit, we use the solutions for the particle trajectory obtained earlier in Eqs. (6a) and (6b),

$$v^{j+1/2} = v_e^{j+1/2} + \frac{q}{m} j \Delta t \, \alpha E^{M+1}(x_e^j), \tag{19a}$$

$$x^j = x_e^j + \frac{q}{m} j \frac{(j-1)}{2} \Delta t^2 \, \alpha E^{M+1}(x_e^j), \tag{19b}$$

where $v_e^{j+1/2}$ and x_e^j are the "explicit" parts of the velocity and position arising from that part of E^* due to $(1-\alpha) E^M$. E^* has been interpolated from the grid to the explicit position x_e^j, which is known. The validity of this approximation is discussed in [5] and requires $|q \Delta t^2 (\partial E/\partial x)/m| \ll 1$, so that the particle advance temporally resolves a trapping oscillation. The implicit orbit-averaged current is Taylor-series expanded with respect to E^{M+1} to obtain

$$\langle J \rangle^{M+1/2} = \langle J_e \rangle^{M+1/2} + \langle \partial J/\partial E^{M+1} \rangle^{M+1/2} E^{M+1}, \tag{20}$$

where $\langle J_e \rangle^{M+1/2}$ is the explicit current given by Eq. (18) with $v^{j+1/2} = v_e^{j+1/2}$ and $x^j = x_e^j$. The functional derivative with respect to E^{M+1} in Eq. (20) operates on $v_i^{j+1/2}$

and x_i^j (which are defined in Eq. (19)) and is evaluated at the explicit velocity and position along the trajectory. The implicit dependence of $\langle J\rangle^{M+1/2}$ on E^{M+1} has thus been linearized, and with the addition of a spatial grid, Eq. (17) leads to a banded-matrix equation whose solution is straightforward. Iterations can be performed in which position x_e^j (at which the electric field is applied) is corrected to include modifications due to E^{M+1}.

The unconditional stability of this scheme for propagating a small-amplitude plasma wave in a cold, uniform, non-drifting plasma follows directly. The analysis is similar to the derivations already presented and is simplified by the absence of corrector iterations. We linearize Eqs. (6), (17), and (18) for a cold, uniform, non-drifting plasma and obtain

$$v^{M+1} = v^M + q\,\Delta T E^*/m, \tag{21a}$$

$$\langle J\rangle^{M+1/2} = n_0 q(v^M + q\,\Delta T E^*/2m), \tag{21b}$$

$$(E^{M+1} - E^M)/\Delta T + (\omega_p^2\,\Delta T E^*/2) + 4\pi n_0 q v^M = 0, \tag{21c}$$

where $E^* = \alpha E^{M+1} + (1-\alpha)E^M$. Fourier analysis and algebraic reduction of these equations give the dispersion relation

$$(z-1)^2 + (\omega_p^2\,\Delta T^2/2)(z+1)(\alpha z + 1 - \alpha) = 0. \tag{22}$$

For $\omega_p^2\,\Delta T^2 \ll 1$, the solution of Eq. (22) is a plasma oscillation

$$\omega^2 \approx \omega_p^2[1 - i(2\alpha - 1)\,\omega\,\Delta T/2)]; \tag{23a}$$

and for $\omega_p^2\,\Delta T^2 \gg 1$,

$$z = (\alpha - 1)/\alpha,\ -1 + (8/(2\alpha - 1)\,\omega_p^2\,\Delta T^2). \tag{23b}$$

All solutions are damped for $\alpha > \frac{1}{2}$.

The general solution of Eq. (22) is unconditionally stable, $|z| \leqslant 1$, for $\alpha \geqslant \frac{1}{2}$. This demonstrates that orbit-averaging can be merged with a direct-particle and field-implicit scheme to give a stable algorithm at large time step, provided that sufficient implicitness is preserved. The failure of a direct-implicit, orbit-averaged algorithm based on Gauss' law (dispersion relation given in Eq. (16)) and the conditional stability of Eq. (22) with respect to α illustrate that stability depends on the particular implicit differencing scheme being used.

A stable algorithm can also be obtained by combining orbit averaging with the implicit moment equation method independently developed in [2] and [3]. In this algorithm, fluid equations for continuity and momentum conservation are introduced,

$$n^{M+1} = n^M - (\Delta T/q)\,D_x J^{M+1/2}, \tag{24}$$

$$J^{M+1/2} = \langle J\rangle^{M-1/2} + (q\,\Delta T/m)(-D_x\langle P^\dagger\rangle^M + qn^M E^*), \tag{25}$$

where $\langle J\rangle^{M-1/2}$ and $\langle P^{\dagger}\rangle^{M}$ are the orbit-averaged current density and kinetic stress. $\langle J\rangle^{M-1/2}$ is given in Eq. (18) with the time average performed over the interval $(M-1)\,\Delta T \leqslant t \leqslant M\,\Delta T$. The orbit-averaged kinetic stress is represented by

$$\langle P^{\dagger}\rangle^{M} = \frac{1}{N+1}\sum_{j=0}^{N}\sum_{i}\frac{m}{2}(v_i^{j+1/2})^2\,[S(x_i^j - x) + S(x_i^{j+1} - x)], \tag{26}$$

and the average is centered on the time interval $(M-\frac{1}{2})\,\Delta T \leqslant t \leqslant (M+\frac{1}{2})\,\Delta T$. The particle equations of motion, Eqs. (2) and (3) are used to advance x and v; Gauss' law

$$D_x E^{M+1} = 4\pi q(n^{M+1} - n_0) \tag{27}$$

determines the electric field. In Eqs. (3) and (25), we choose to represent the electric field as

$$E^{*} = \theta E^{M+1} + ((1-\theta)/4)(E^{M+1} + 2E^{M} + E^{M-1}), \tag{28}$$

where $0 \leqslant \theta \leqslant 1$. The value $\theta = 0$ corresponds to a centered-implicit scheme, and $\theta = 1$ is fully implicit.

Figure 3 illustrates the time advance of the various fluid and particle quantities. Because a field solve is performed to obtain E^{M+1} before the particles are advanced from $M\,\Delta T$ to $(M+1)\,\Delta T$ and this field solution requires an evaluation of $\langle P^{\dagger}\rangle^{M}$ in Eq. (25) that is not completely known (particle velocity and position data from $M\,\Delta T$ to $(M+\frac{1}{2})\,\Delta T$ are not yet determined), extrapolation or prediction of $\langle P^{\dagger}\rangle$ is necessary in Eq. (25). For example, on a field predictor pass, it is convenient to set $\langle P^{\dagger}\rangle$ equal to $\langle P^{\dagger}\rangle^{M-1/2}$ in Eq. (25). We can then calculate E^{M+1} and advance the particles from $M\,\Delta T$ to $(M+\frac{1}{2})\,\Delta T$ so that $\langle P^{\dagger}\rangle^{M}$ can be computed and used to recalculate E^{M+1}, which is then used to advance the particles from $M\,\Delta T$ to $(M+1)\,\Delta T$. It has been the experience in the work reported in [2–4] that considerable liberties can be taken in the evaluation of $P^{\dagger}$ with respect to time centering. As initial conditions in our orbit-averaged schemes, we assume that the plasma is frozen for $t \leqslant 0$ and then set all the orbit-averaged particle data and fluid quantities equal to the corresponding instantaneous particle quantities at $t = 0$.

The stability analysis for plasma oscillations in the orbit-averaged, moment-equation scheme is straightforward and closely follows the pattern of the similar

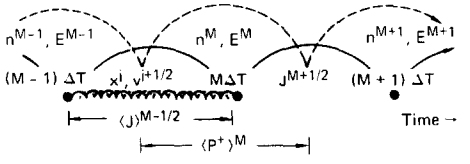

FIG. 3. Time advance of fluid and particle variables in the orbit-averaged, implicit-moment equation method.

derivations that have already appeared in this section. The linearized, algebraically reduced difference equations for a cold, uniform plasma are derived directly from Eqs. (2), (3), (24)–(28), and (18):

$$v^{M+1} - v^M = q\,\Delta T\,E^*/m, \tag{29a}$$

$$J^{M+1/2} = \langle J\rangle^{M-1/2} + q^2 n_0\,\Delta T\,E^*/m = n_0 q(v^{M-1} + v^M)/2 + q^2 n_0\,\Delta T\,E^*/m, \tag{29b}$$

$$qn^{M+1} = qn^M - \Delta T\,D_x J^{M+1/2}, \tag{29c}$$

$$D_x E^{M+1} = 4\pi q(n^{M+1} - n_0). \tag{29d}$$

There is no corrector iteration here because a linear plasma oscillation in a cold, non-drifting plasma has no associated kinetic stress. Use of Eq. (28), Fourier analysis of Eq. (29), and algebraic reduction yields the quartic dispersion relation

$$z^2(z-1)^2 + \omega_p^2\,\Delta T^2(z^2 - \tfrac{1}{2}z + \tfrac{1}{2})\left[\theta z^2 + \frac{(1-\theta)}{4}(z^2 + 2z + 1)\right] = 0. \tag{30}$$

For very small time steps (or low frequencies) $\omega_p^2\,\Delta T^2 \ll 1$, there are heavily damped solutions

$$z \approx \pm i(1-\theta)\,\omega_p\,\Delta T/8, \tag{13a}$$

and a simple-harmonic oscillation

$$\omega \approx \pm\omega_p[1 \pm i(1-2\theta)\,\omega_p\,\Delta T/4], \tag{31b}$$

which is damped if $\theta > \frac{1}{2}$. For $\omega_p^2\,\Delta T^2 \gg 1$, the plasma oscillations become significantly damped

$$z = \tfrac{1}{4} \pm i\sqrt{7}/4, \qquad |z| = \sqrt{2}/2, \tag{32a}$$

and the remaining solutions are

$$z = (-1 + \theta \pm i2[\theta(1-\theta)]^{1/2})/(1 + 3\theta). \tag{32b}$$

which are also damped when $0 \leqslant \theta \leqslant 1$. Figure 4 exhibits the absolute value of the amplification factor $|z|$, the solution of Eq. (30), as a function of $\omega_p^2\,\Delta T^2$. We note that for insufficient implicitness $\theta < \frac{1}{2}$, there is instability; but, curiously, the instability occurs at small and moderate values of $\omega_p\,\Delta T$ and not at large $\omega_p\,\Delta T$. Setting $\theta \geqslant \frac{1}{2}$ assures stability for all values of $\omega_p\,\Delta T$.

The next model that we analyze is a variation of the orbit-averaged moment method in which we attempt to tie the fluid moments closer to their corresponding orbit-averaged particle quantities. In the scheme already described, the fluid and the particles are coupled by using the orbit-averaged particle current and kinetic stress in Eq. (25), by sharing the same initial data for the number density, current, and stress tensor, and by being advanced with the same electric field E^* in Eqs. (3) and (25).

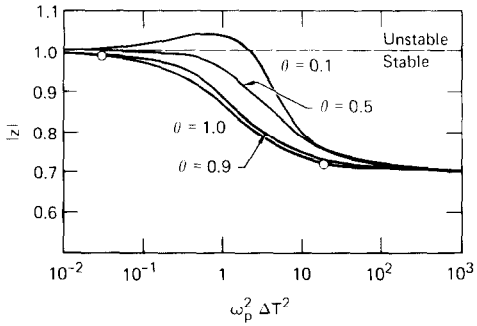

FIG. 4. Absolute value of the amplification factor $|z|$ for electron plasma oscillations as a function of $\omega_p^2 \Delta T^2$ for the orbit-averaged, implicit moment equation method. Simulation data points are superposed.

A simple modification of Eqs. (24)–(27) that couples the fluid and particles more closely is the addition of a step in which the fluid density is replaced by

$$n^{M+1} = n^M - \Delta T\, D_x \langle J \rangle^{M+1/2}/q \tag{33}$$

following the field solution in Eq. (27). This seemingly minor change in the algorithm has a profound effect and results in instability. It is important not to confuse the distinction between n^{M+1} calculated in Eq. (24) and used in determining E^{M+1} in Eq. (27), and n^{M+1} obtained in Eq. (33) and then used on the right side of Eq. (24)

Fourier analysis of the modified difference equations and algebraic reduction yields

$$z^3(z-1)^2 + \omega_p^2 \Delta T^2 [z^2 + \tfrac{1}{2}z - \tfrac{1}{2} + z(z-1)^2] \times [\theta z^2 + ((1-\theta)/4)(z^2 + 2z + 1)] = 0. \tag{34}$$

For $\omega_p^2 \Delta T^2 \ll 1$, there are heavily damped solutions

$$z = (\tfrac{1}{2}, \tfrac{1}{4} \pm i\sqrt{3}/4)(\omega_p \Delta T)^{2/3}\,(1-\theta)^{1/3} \tag{35}$$

and plasma oscillations

$$\omega = \pm\omega_p[1 \pm i(\omega_p \Delta T/4)(1-2\theta)], \tag{36}$$

which are damped for $\theta > \frac{1}{2}$ just as in Eq. (31b). For $\omega_p^2 \Delta T^2 \gg 1$, the normal modes are approximately described by setting the two brackets appearing in Eq. (34) separately equal to zero. The cubic has two solutions corresponding to unstable plasma oscillations,

$$z = 0.3017 \pm i1.0815, \qquad |z| = 1.123, \tag{37a}$$

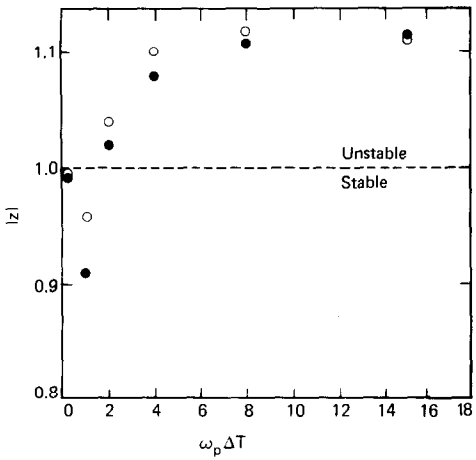

FIG. 5. Absolute value of the amplification factor $|z|$ for plasma oscillations as a function of $\omega_p \Delta T$ for the unstable, modified, orbit-averaged, implicit-moment equation method using Eq. (33). O, theory; ●, simulation.

and a damped solution,

$$z = 0.3966; \tag{37b}$$

the two solutions of the quadratic are stable for $0 \leqslant \theta \leqslant 1$,

$$z = (-1 + \theta \pm i2[\theta(1-\theta)]^{1/2})/(1 + 3\theta). \tag{37c}$$

Figure 5 illustrates the solution of Eq. (34) for $\theta = 1$; which corresponds to a fully implicit scheme. The amplification factor $|z|$ is less than unity, and the plasma oscillation is damped for $\omega_p \Delta T \leqslant \mathcal{O}(1)$. The plasma oscillation becomes unstable at larger time steps.

Another variation of Eqs. (24)–(27) consists of replacing Eq. (24) with

$$n^{M+1} = \langle n \rangle^M - \Delta T D_x J^{M+1/2}/q. \tag{38}$$

This can be implemented by calculating $\langle n \rangle^M$ in the same predictor–corrector iteration in which $\langle P^\dagger \rangle^M$ is computed. However, linear stability analysis indicates that violent numerical instability results for $\omega_p \Delta T > 1$.

Mason [9] has suggested that Eqs. (24) and (25) could be replaced by

$$n^{M+1} = \langle n \rangle^{M-1/2} - 3\Delta T D_x J^{M+1/2}/2q \tag{39}$$

$$J^{M+1/2} = \langle J \rangle^{M-1/2} + q\,\Delta T(-D_x \langle P^\dagger \rangle^M + qnE^*)/m. \tag{40}$$

This increases the implicit dependence of n^{M+1} on E^{M+1}. We have analyzed the linear stability of Eqs. (2), (3), (27), (39), and (40) with E^* in Eqs. (3) and (40)

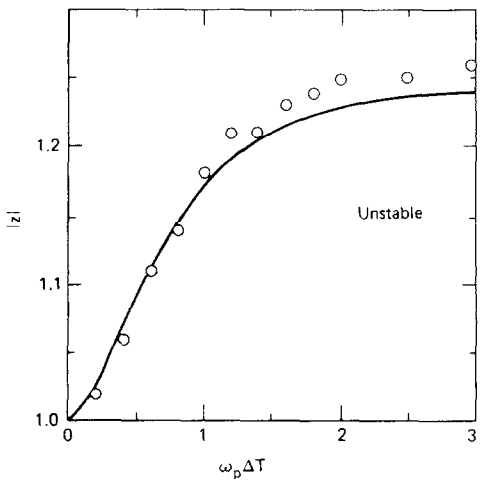

FIG. 6. Absolute value of the amplification factor $|z|$ for plasma oscillations as a function of $\omega_p \Delta T$ for the unstable, modified, orbit-averaged implicit-moment equation method using Eqs. (39) and (40). O, simulation data.

represented by different weighted averages of E^{M+1}, E^M, and E^{M-1}. We found instability for some range of $\omega_p \Delta T$ values in every case. As an example, in Fig. 6 we present the absolute value of the amplification factor $|z|$ as a function of $\omega_p \Delta T$ for a scheme in which E^* in Eq. (3) was the simple average $(E^M + E^{M+1})/2$ and E^* in Eq. (40) was E^{M+1}.

It is evidently difficult to marry the fluid density any closer to the orbit-averaged particle data than is already accomplished in Eqs. (24) and (25) without compromising numerical stability. For the sake of numerical stability, we favor the use of Eqs. (24)–(27) with $\theta \geqslant \frac{1}{2}$. We next ask:

(a) What are the accuracy properties of such an algorithm?

(b) What discrepancies between fluid and particle quantities are expected?

2.2. *Accuracy*

We have performed a standard accuracy analysis in which the density and current are Taylor-series expanded with respect to temporal and spatial variation. We presume that all spatial derivatives are represented by the simplest centered difference operators and hence, are accurate through first order in Δx, with errors at second order. The equation for the current, Eq. (25), is centered in space but not in time. $\langle P^\dagger \rangle^M$ is approximately time centered in a predictor–corrector sense; with one corrector pass, it is accurate up to $\mathcal{O}(\Delta T)^2$. With a fully implicit representation of E^*, rather than centered implicit, there is an $\mathcal{O}(\Delta T)$ error in the electric field used in Eq. (25). Because $J^{M+1/2}$ is only one macro-time step ahead of the orbit-averaged particle data $\langle J \rangle^{M-1/2}$, however, the first-order error in E^* is multiplied by an

additional ΔT to give a net $\mathcal{O}(\Delta T^2)$ error in $J^{M+1/2}$. With centered differencing and linear interpolation, the particle equations (2) and (3) have similar accuracy properties and are advanced with the same E^*. Thus, the discrepancy $J^{M+1/2} - \langle J \rangle^{M+1/2}$ is at most second order in ΔT and Δx. Similarly, as a consequence of centered differencing, the discrepancy $n^{M+1} - \langle n \rangle^{M+1}$ is also at most second order in ΔT and Δx.

If a stable algorithm could be constructed using Eq. (38), the discrepancy $n^{M+1} - \langle n \rangle^{M+1}$ would be $\mathcal{O}(\Delta T)$ smaller, because n^{M+1} is advanced only one time step ahead of $\langle n \rangle^M$. Whether the accuracy of the stable scheme using Eqs. (24) and (25) is sufficient will have to be determined in practice and may well depend on the pathology of the particular problem. The absolute accuracy of the orbit-averaged, direct-particle, and field-implicit method is generally at least as good as in the implicit moment method; in contrast, there are no fluid quantities introduced, and discrepancies between the density used in Poisson's equation and the actual particle number density are of a different character [5].

3. Simulation Results

The one-dimensional electrostatic particle code ES1 [8] was used as a framework to test various differencing schemes. In all cases there was no magnetic field present. The results reported in [2–5] demonstrate the successful implementation of implicit time differencing in electrostatic algorithms. Our experience with orbit averaging in electrostatic models has been successful in a limited sense.

As analyzed in Section 2.1, orbit averaging alone in explicit electrostatic and hybrid quasi-neutral schemes gave numerical instability. No amount of uncentering in the difference equations or additional corrector iterations achieved stability in our simulations, in agreement with the analysis of Section 2.1.

The introduction of sufficient implicitness led to stable algorithms. Examples of schemes based on the implicit-moment method [2, 3] with insufficient implicitness were described in Section 2.1. Simulations of numerically unstable electron plasma oscillations in cold plasma were in good agreement with the relevant dispersion relations (see Figs. 5 and 6). Simulations using the version of the orbit-averaged implicit-moment method described in Eqs. (2), (3), (18), and (24)–(28) gave damped plasma oscillations for small and large $\omega_p \Delta T$ in good agreement with the solutions of the dispersion relation Eq. (30) and plotted in Fig. 4. For these cold plasma simulations of small amplitude waves, only a predictor step was used, because corrector iterations would have only modified the stress term $\langle P^\dagger \rangle$, which was unimportant in these situations.

A more substantial test of the electrostatic algorithms was the simulation of an ion acoustic wave. In this case the electrons were warm, and the ions were cold. The results of single mode simulations are shown in Figs. 7–9. The particular mode simulated had quite long wavelength $k\lambda_{De} = 0.5 \times 10^{-2}$ and hence, low frequency $kc_s/\omega_{pe} = 10^{-3}$. The mass ratio was $m_i/m_e = 25$, and the other simulation parameters

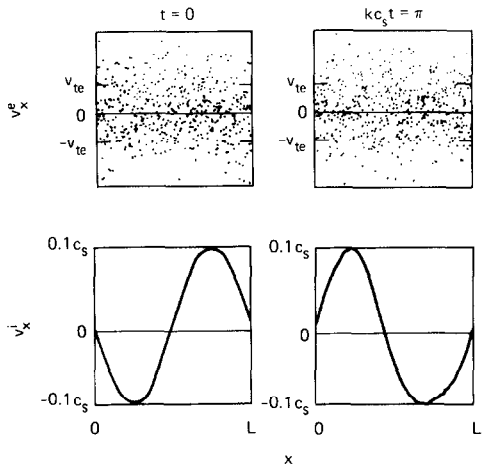

FIG. 7. Electron and ion phase space v_x vs x for a periodic ion acoustic-wave simulation at $kc_s t = 0$ and π with 512 particles of each species. The system length is L, and c_s is the ion sound speed.

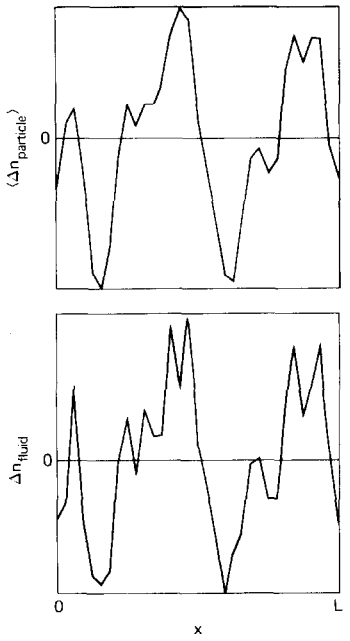

FIG. 8. Orbit-averaged and fluid perturbed number densities $\Delta n \equiv n_i - n_e$ as functions of x at $kc_s t = 4\pi$, corresponding to 3×10^3 macro-time steps with $\Delta T/\Delta t_e = 20$ and $\Delta t_e = \Delta t_i$ for the same periodic ion acoustic-wave simulation shown in Fig. 7. The relative ion (or electron) density perturbation satisfied $|(n_i - n_0)/n_0| \leqslant 0.1$.

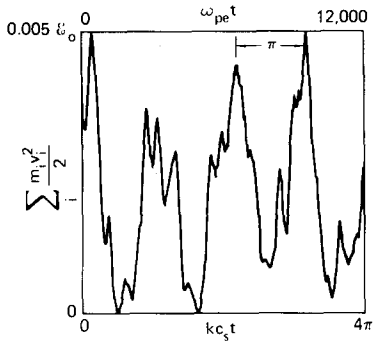

FIG. 9. For the same periodic ion acoustic-wave simulation shown in Fig. 8, ion kinetic energy vs time, where $\mathscr{E}_0$ is the total system energy (conserved within 1%).

were $\omega_{pe}\Delta T = 4$, $kv_e\Delta T = 0.02$, $\Delta T/\Delta t = 20$, $\Delta t_e = \Delta t_i$, and $N_i = N_e = 512$; there were 32 grid cells. One corrector iteration was performed.

The results of the simulations clearly show an ion-acoustic standing wave with correct frequency (Figs. 7 and 9), nearly constant total energy after 6×10^4 particle time steps ($\leqslant 1\%$ variation), and little separation of the orbit-averaged particle density from the fluid density (Fig. 8). Spatial smoothing was applied to the calculated electric field, and only the fundamental was retained. Consistent spatial smoothing, a problem in the implicit algorithms described here, is currently unresolved. Nevertheless, the small separation of the fluid and particle densities, especially in the mode of interest, is encouraging in view of the relatively few particles (512 of each species) used.

An important and discouraging result of the orbit-averaged, electrostatic implicit-moment simulations is their observed divergence for $kv_e\Delta T \gtrsim 0.1$. The empirically determined stability is more restrictive than is imposed by the moment method with no orbit averaging, where $kv\Delta t < 1$. However, because of the artifical cooling–heating and general distortion of the particle orbits that accompanies use of $kv\Delta t \geqslant \mathscr{O}(1)$ in any particle code [11], use of $kv_e\Delta T \lesssim 0.1$ in the orbit-averaged code may prove to be a factor at most 2 to 4 times more restrictive than that of the typical time step used in conventional implicit moment method simulations. In any case, in its present configuration, the orbit-averaged implicit moment algorithm does *not* achieve a reduction in the total operations count over simulations with the conventional implicit moment method. The orbit averaging does reduce the number of simulation particles, however, and, hence, decreases the computer memory requirement.

We emphasize that these results only apply to the particular algorithm used here with its explicit representation of the kinetic stress term. Better convergence properties and less restrictive conditions on time step should result in Eq. (25) if an implicit or partially implicit representation of the kinetic stress tensor is introduced [4, 10] and/or the orbit-averaged current $\langle J\rangle^{M-1/2}$ is replaced with the fluid quantity

$J^{M-1/2}$. Our limited success with orbit averaging in the electrostatic model has provided insights regarding the right conditions for successful application of orbit averaging, which we shall discuss in Section 4.

We have had some success with another form of temporal averaging in an almost trivial variation of the implicit moment method. As conceived by Mason [2] and Denavit [3] the charge density, current density, and kinetic stress terms on the right sides of the moment equations (24) and (25) were to be obtained from the instantaneous particle quantities accumulated on the spatial grid; there was no splitting of field-solve and particle-advance time scales. We performed temporal smoothing of the particle source data in the moment equations without time splitting by introducing simple lag averages,

$$\overline{P^{\dagger M}} = \alpha_1 P^{\dagger M} + (1-\alpha_1)\,\overline{P^{\dagger M-1}},$$
$$\overline{J}^{M-1/2} = \alpha_2 J^{M-1/2} + (1-\alpha_2)\,\overline{J}^{M-3/2},$$
$$\bar{n}^M = \alpha_3 n^M + (1-\alpha_3)\,\bar{n}^{M-1},$$

where $0 \leqslant \alpha_i \leqslant 1$; the barred quantities are the average values at a particular time level, and the remaining quantities are the respective instantaneous values. The time average extends backward in time, has a dissipative effect, and can be destabilizing depending on the values of $\{\alpha_i\}$ and $\omega_{pe}\,\Delta t$. To ensure stability at large ω_{pe}, we have found that α_3 has to be set nearly equal to unity (no averaging of n), and successively smaller values of α_2 and α_1 (more averaging of past J and $P^\dagger$ data) can be taken. This does not achieve dramatic reduction of the particle statistical requirement but does decrease statistical noise.

4. Discussion and Summary

The foregoing analysis and simulations demonstrate that orbit averaging and implicit techniques can be merged to give new algorithms that are stable for large time steps; this is not possible with conventional explicit-particle codes. In so doing, however, we have also discovered numerous schemes that were numerically unstable either at small or large time steps. Furthermore, the electrostatic and magneto-inductive models have entirely different characteristics. Orbit averaging has been very successful in the magneto-inductive model with an applied magnetic field present but has been less successful in the unmagnetized electrostatic model.

In general, orbit averaging can lead to numerical instability, unless it is combined with sufficient *implicitness*. The *explicit* orbit-averaged, magneto-inductive scheme first introduced in [1] and further described in the companion paper has peculiar properties and is unstable for some parameter regimes and small ΔT. Because it is highly desirable to have robustly stable algorithms that are applicable to diverse parameter regimes, we prefer to combine orbit averaging with implicit schemes such as those described in [2–5] and in this article. Therefore, we are adding orbit

averaging to an axisymmetric cylindrical version of an electromagnetic implicit moment code similar to that developed by Brackbill and Forslund [4].

Although we were able to construct a stable, orbit-averaged electrostatic scheme, such a code did not prove to be as successful an application of orbit averaging in its present configuration as hoped. This is due to the lack of separation of time scales between the time step required for stability of the field solution and the natural time step for the particle advance, in sharp contrast to the situation for the magneto-inductive algorithm. The constraint on the time step for the field solution in the electrostatic implicit moment method is approximately

$$|kv\,\Delta T| < 1 \tag{41}$$

in an unmagnetized plasma, where k is the largest wave number retained, and v is the larger of the thermal and mean oscillation or drift velocities [2, 3].

The constraint condition, Eq. (41), is the inevitable consequence of the explicit representation of the kinetic stress term and the structure of the implicit moment equations. Iterations on the kinetic stress term and the electric field solution are coupled, and Denavit [3] has shown that the convergence condition on the iteration of the moment equations is given by Eq. (41). A perturbation in the kinetic stress $\delta P^{\dagger M}$ is induced by changes in the particle trajectories resulting from changes in the electric field δE^{M+1}. To determine the convergence of iterations, one calculates the ratio of the perturbations δE^{M+1} on successive iterations, i.e., $|\delta E_{r+1}^{M+1}/\delta E_r^{M+1}|$, where r is the iteration index. Depending somewhat on the specific finite-difference representation of the stress tensor and the shape of the unperturbed velocity distribution function, the perturbation in the $r+1$ iterant of the stress tensor is given by

$$\delta P_{r+1}^{\dagger M} = -i\gamma n_0 m v^2 k\,\Delta t^2\, q(\partial E^*/\partial E^{M+1})\,\delta E_r^{M+1}, \tag{42}$$

where $\gamma = \mathcal{O}(1)$, v is a characteristic thermal velocity, and $\partial E^*/\partial E^{M+1}$ is determined from Eq. (28), for example. Equation (25) relates $\delta J_{r+1}^{M+1/2}$ to $\delta P_{r+1}^{\dagger M}$ and to the implicit term δE_{r+1}^{M+1}. The density perturbation δn_{r+1}^{M+1} is determined by $\delta J_{r+1}^{M+1/2}$ in Eq. (24). Gauss' law, Eq. (27), closes the set of equations by relating the electric field and charge–density perturbations $ik\,\delta E_{r+1}^{M+1} = 4\pi q \delta n_{r+1}^{M+1}$. Finally, we obtain

$$\left|\frac{\delta E_{r+1}^{M+1}}{\delta E_r^{M+1}}\right| = \left|\frac{\gamma k^2 v^2\,\Delta T^2\,\omega_p^2\,\Delta T^2\,\partial E^*/\partial E^{M+1}}{1+\omega_p^2\,\Delta T^2\,\partial E^*/\partial E^{M+1}}\right|. \tag{43}$$

Using the property that $\partial E^*/\partial E^{M+1} > 0$ in all of our implicit schemes, we conclude that $|\delta E_{r+1}^{M+1}/\delta E_r^{M+1}| < 1$ for all $\omega_p^2 \Delta T^2$ if $\gamma k^2 v^2 \Delta T^2 < 1$; this is in basic agreement with Eq. (41).

Note that Eq. (41) is essentially the same condition as that for accurate integration of the particle equations of motion. When we attempt to orbit average, we are forced to use a Δt for the particle advance much less than ΔT for the field, in which time a typical particle does not traverse much of its available phase–space trajectory. Orbit averaging was successful in the magneto-inductive case because the particles were

able to complete many gyro- and axial-bounce orbits over the macro-step ΔT between field solves, while being simultaneously constrained to use a micro step Δt fine enough to accurately resolve the gyration and the bouncing. In the unmagnetized electrostatic model, the analogue of the gyro- or axial-bounce orbit is the wavelength of the electric field. Thus, the inequality in Eq. (41) is just the reverse of that which would have allowed orbit averaging to achieve maximal improvement of code efficiency.

Orbit averaging of the implicit moment algorithm with explicit pressure has not reduced the total number of operations in simulations with no magnetic field. However, the number of particles is reduced. The memory requirements and/or the input–output costs for particle data stored on disk are consequently lessened. Furthermore, as pointed out by Adam *et al.*, [12], in orbit averaging the particle advance over the many micro-time steps comprising a full macro-time interval can be independently completed for each particle. Economies in computations accrue from the large reduction in information retrieval from the string of particle data.

Mason, Brackbill, and Forslund have been successful in relaxing the $|kv\,\Delta T| < 1$ constraint on the convergence of the conventional implicit moment method by introducing implicitness into the prescription for the stress tensor [2, 4]. This should be helpful in establishing the necessary separation of micro- and macro-time scales required for orbit averaging. With $kv\,\Delta t \lesssim 0.2$ to accurately resolve the particle orbits and $kv\,\Delta T \gtrsim \mathcal{O}(1)$, orbit averaging would be more efficacious.

Orbit averaging of the direct implicit particle code ought to be successful for systems in which the electric fields are weak. The time-step constraint for the direct implicit solution is

$$kv_{\mathrm{tr}}\,\Delta T = (e\phi/T)^{1/2}\,kv_{\mathrm{t}}\,\Delta T < 1,$$

where $v_{\mathrm{tr}} \equiv (e\phi/m)^{1/2}$ is the trapping velocity and $v_{\mathrm{t}} = (T/m)^{1/2}$ is the thermal velocity. If the electric fields are weak, i.e., if $e\phi \ll T$, then $kv_{\mathrm{tr}}\,\Delta T \ll kv_{\mathrm{t}}\,\Delta T$; and the constraint on the field-solution time step is much less stringent than that for accurate particle pushing ($kv_{\mathrm{t}}\,\Delta t < 1$). Hence, there arises the necessary separation of time scales needed for orbit averaging to be successful. This has been recognized by Adam *et al.*, in their discussion of "sub-cycling" [12].

For wave propagation perpendicular to an applied magnetic field, the convergence constraint on the implicit moment equations differs considerably from Eq. (41). To accommodate a magnetic field, the right side of Eq. (25) acquires the additive term

$$(\Delta T/2mc)(\mathbf{J}^{M+1/2} + \mathbf{J}^{M-1/2}) \times \mathbf{B}^{M}, \tag{44}$$

where $J^{M-1/2}$ could be the old value of either the instantaneous particle current density, the orbit-averaged current density, the fluid current density, or some linear combination of these. The $\mathbf{v} \times \mathbf{B}$ force is added similarly to the particle equations of motion as in [1] and the companion paper. The implicit solution of Eq. (25) for $\mathbf{J}^{M+1/2}$ as a *linear* function of E^* is obtained with the standard Boris or Buneman method and is stable for arbitrary value of $\omega_{\mathrm{c}}\,\Delta T$ [8].

We have performed an analysis of the convergence of a model $\mathbf{P}^+$-iteration scheme including a magnetic field. The analysis is similar to that which leads to Eqs. (42) and (43) but is complicated by the addition of the $\mathbf{v} \times \mathbf{B}$ force in the particle equations of motion and the $\mathbf{J} \times \mathbf{B}$ force in the moment equations. The magnetic field also adds several new physical time scales, e.g., the cyclotron frequency harmonics, the diamagnetic drift frequency, and the ∇B and curvature drift frequencies, all of which influence perpendicular wave propagation. We find that high-frequency waves ($\omega \geqslant |\omega_c|$) can be suppressed with implicit differencing and filtering [e.g., $\theta > 0$ in Eq. (28)]. The stability of the remaining long-wavelength, low frequency electrostatic waves is determined by the convergence of iterations on the kinetic stress term, but is

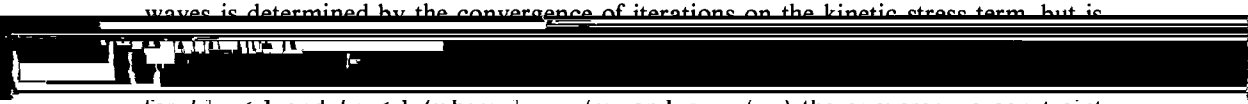

for $k\lambda_D < 1$ and $ka < 1$ (where $\lambda_D \equiv v/\omega_p$ and $a = v/\omega_c$) the convergence constraint can be made much less severe than the time-step constraint on accurate particle pushing in the magnetic field $|\omega_c \Delta t| < 1$. This separation of time scales $\Delta t \ll \Delta T$ creates a more promising situation for orbit averaging than in the unmagnetized case with an explicit stress tensor.

Accuracy considerations should receive more attention than we have given here. We have made virtually exclusive use of difference schemes whose electric field representation was uncentered and not second-order accurate with respect to time step, e.g., Eq. (28) for $\theta \neq 0$. This was motivated by the desire for simplicity in both the analysis and the presentation; our first priority was given to constructing numerically stable schemes. On the whole, our simulation experience with first-order schemes and that of Mason [2] have been satisfactory. Difference schemes of higher-order accuracy, however, are desirable and can be designed. Cohen *et al.*, [11] have investigated the accuracy and stability of various implicit schemes in detail.

It is clear from this study and those reported in [2–5] that the invention of implicit algorithms has led to significant gains in the problem of large time steps in particle simulations, and large economies in computations have been achieved as a result. In some circumstances, smoothing of statistical noise and additional savings in computations and/or computer memory requirements can be obtained by the use of time-splitting and orbit-averaging techniques in combination with the implicit methods as described here. In this last regard, there seems to be room for further development.

ACKNOWLEDGMENTS

We are pleased to acknowledge and thank C. K. Birdsall, J. U. Brackbill, J. A. Byers, J. Denavit, D. W. Forslund, A. Friedman, A. B. Langdon, and R. J. Mason for many helpful discussions, assistance, interest, and encouragement. B. I. Cohen thanks J. R. Albritton for numerous valuable criticisms, his perceptive comments regarding the importance of a magnetic field in establishing multiple time scales, and his steadfast skepticism that gave considerable impetus to this endeavor.

This document was prepared as an account of work sponsored by an agency of the United States Government. Neither the United States Government nor the University of California nor any of their

REFERENCES

1. B. I. COHEN, T. A. BRENGLE, D. B. CONLEY, AND R. P. FREIS, *J. Coput. Phys.* **38** (1980), 45.
2. R. J. MASON, *J. Comput. Phys.* **41** (1981), 233.
3. J. DENAVIT, *J. Comput. Phys.* **42** (1981), 337.
4. J. U. BRACKBILL AND D. W. FORSLUNG, *J. Comput. Phys.*, to appear.
5. A. FRIEDMAN, A. B. LANGDON, AND B. I. COHEN, *Comments Plasma Phys, Controlled Fusion* **6** (1981), 225.
6. R. P. FREIS, *Nucl. Fusion* **13** (1973), 247.
7. B. I. COHEN AND R. P. FREIS, *J. Comput. Phys.* **45** (1982), 367.
8. C. K. BIRDSALL AND A. B. LANGDON, "Plasma via Computer Simulation," McGraw–Hill, New York, to appear.
9. A. B. LANGDON, *J. Comput. Phys.* **30** (1979), 202.
10. R. J. MASON, private communication, 1981.
11. B. I. COHEN, A. B. LANGDON, AND A. FRIEDMAN, *J. Comput. Physics*, to appear.
12. J. C. ADAM, A. GOURDIN SERVENIERE, AND A. B. LANGDON, "Electron Subcycling in Particle Simulation of Plasmas," École Polytechnique Rep., Palaiseau, France, 1981; *J. Comput. Physics*, submitted.